Journal of Neuroscience Methods 274 (2016) 164–171

Contents lists available at ScienceDirect

Journal of Neuroscience Methods

journal homepage: www.elsevier.com/locate/jneumeth

Optical coherence tomography based microangiography provides an ability to longitudinally image arteriogenesis *in vivo*

Yuandong Li[a], Woo June Choi[a], Wan Qin[a], Utku Baran[a,b], Lauren M. Habenicht[c], Ruikang K. Wang[a,*]

[a] Department of Bioengineering, University of Washington, Seattle, WA, USA
[b] Department of Electrical Engineering, University of Washington, Seattle, WA, USA
[c] Department of Comparative Medicine, University of Washington, Seattle, WA, USA

HIGHLIGHTS

- OCT/OMAG reveals collateral vessel morphology change, blood flow velocity and directionality change over a longitudinal study in small animal models.
- Growth phase of arteriogenesis, confirmed by OCT/OMAG imaging, occurs between 12 and 24 h after blood flow obstruction.
- Local inflammation accompanied by arteriogenesis is presented by tissue thickness change and lymphatic vessel formation in mouse ear.
- An activation of the collateral flow at arteriolo-arteriolar anastomoses (AAA) in mouse brain is observed during MCAO.

GRAPHICAL ABSTRACT

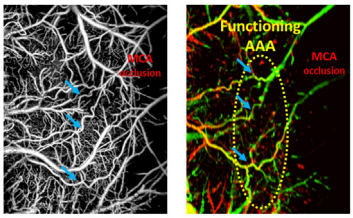

Monitoring arteriogenesis at the cerebral arteriolo-arteriolar anastomoses (AAAs) in mouse brain during middle cerebral artery occlusion using OCT-based microangiography (OMAG) (left) and Doppler OMAG (right).

ARTICLE INFO

Article history:
Received 16 August 2016
Received in revised form 11 October 2016
Accepted 13 October 2016
Available online 14 October 2016

Keywords:
Optical coherence tomography
OCT angiography
Arteriogenesis
Collateral circulation
Occlusive vascular disease
Stroke

ABSTRACT

Background: Arteriogenesis describes the active growth of the pre-existing collateral arterioles, which is a crucial tissue-saving process in occlusive vascular diseases.
New method: We propose to use optical coherence tomography (OCT)-based microangiography (OMAG) to monitor arteriogenesis following artery transection in mouse ear and focal stroke in mouse brain.
Results: Our longitudinal mouse ear study shows that the growth phase of arteriogenesis, indicated by changes in collateral vessel diameter and velocity, occurs between 12 and 24 h after vessel transection. Additionally, the magnitude of local inflammation is consistent with the time course of arteriogenesis, judging by the tissue thickness measurement and lymphatic vessel signals in OCT. In the mouse brain study, collateral vessel morphology, blood flow velocity and directionality are identified, and an activation of the collateral flow at the arteriolo-arteriolar anastomoses (AAA) is observed during stroke.
Comparison with existing methods: In comparison with histology and fluorescence imaging, OCT/OMAG is completely non-invasive and capable of producing consistent results of longitudinal changes in collateral vessel morphology and vasodynamics.

* Corresponding author at: Biophotonics and Imaging Laboratory, Department of Bioengineering, University of Washington, 3720 15th Ave NE, N415A, Seattle, WA, USA.
E-mail address: wangrk@uw.edu (R.K. Wang).

http://dx.doi.org/10.1016/j.jneumeth.2016.10.010

Conclusion: OCT/OMAG is a promising imaging tool for longitudinal study of collateral vessel remodeling in small animals. This technique can be applied in guiding the *in vivo* experiments of arteriogenesis stimulation to treat occlusive vascular diseases, including stroke.

1. Introduction

Collateral arterioles are interconnected with arteriolo-arteriolar anastomoses (AAA) in highly vascularized organs, such as heart, skin, and brain (van Royen et al., 2001; Toriumi et al., 2009). In the case of blood flow obstruction, collateral arterioles are able to grow into larger conductive arteries by active proliferation of vascular endothelial and smooth muscle cells (Heil et al., 2006; Schaper and Buschmann, 1999). The adaptive growth of collateral vessels, termed "arteriogenesis", is crucial for maintaining regional blood supply and offsetting the adverse effect of tissue ischemia (Liu et al., 2014). Recently, stimulation of arteriogenesis has become a popular candidate for the treatment of occlusive vascular diseases, such as peripheral arterial disease (PAD) (van Royen et al., 2001). Hence, an ability to monitor progressive development of collateral vessels is essential to better understand the mechanisms of arteriogenesis and evaluate the effectiveness of stimulation therapies.

There are three phases in arteriogenesis: initiation, growth, and maturation (Meisner and Price, 2010). In each phase, the targeted collateral arterioles undergo different magnitudes of vessel remodeling, resulting in increased diameter and blood flow. The first phase occurs immediately after blood flow obstruction, when a drop in perfusion pressure at one side of the collateral arteriole causes a shear stress change on the collateral vessel wall. It immediately initiates a complex cascade of molecular and cellular events, leading to endothelium activation (Heil et al., 2006). The growth phase occurs between 12 and 24 h after the initial occlusion (Buschmann et al., 2003). During this period, recruitment of monocytes further stimulates endothelial and smooth muscle cell proliferation and facilitates extracellular matrix breakdown, which allows the vessel to expand in size. After 24 h, proliferation wanes and the collateral arteriole either matures into a conductive artery or goes through regression. An ability to reveal the detailed vascular dynamics *in vivo* at each phase would be critical to guide the experimental design of arteriogenesis stimulation.

Other arteriogenic factors, such as inflammation, plays a pivotal role in arteriogenesis to ensure the releasing of growth factors, proteases for structural remodeling (Schaper and Scholz, 2003). Previous studies have shown that an infusion of monocyte chemoattractant factor MCP-1 (CCL2) produced a 4-fold increase of collateral growth after femoral artery occlusion in rabbits (Buschmann et al., 2001). From this perspective, evaluating local inflammatory response will improve our understanding of arteriogenesis mechanism and evaluate inflammation-regulated collateral growth.

To investigate vessel remodeling during arteriogenesis, histological analysis is often used to assess vessel morphology (Schaper and Scholz, 2003; Demicheva et al., 2008; North and Sanders, 1958). While promising, this approach is limited to a single time point in each individual, and cannot evaluate dynamic changes in collateral arterioles over time. It is therefore desirable to use a non-invasive *in vivo* imaging technology to study the process of arteriogenesis. Laser speckle perfusion imaging (LSI) has been explored to reveal the dynamic change in the cortical collateral circulation in rodent models during acute ischemic stroke (Wang et al., 2012). However, the spatial resolution of LSI is inadequate to visualize the detailed collateral remodeling of small vessels within localized regions. Two-photon excited fluorescence microscopy (TPM) is an alternative method that provides highly detailed microvascular structure (Schaffer et al., 2006), but the small field of view provided by TPM sometimes fails to capture a collateral vessel of interest. Photoacoustic imaging (PA) is a newly developed technique, which has emerged in the past decade as a powerful hybrid imaging modality for detailed vascular imaging in various tissue types (Hu et al., 2009). Nevertheless, the requirement of contact with tissue during measurement can confound the measurement of blood flow (Qin et al., 2015, 2016).

In vivo imaging technology has also been used for evaluating tissue inflammation. TPM has been used to observe the dynamics of immune cells labeled with fluorescent proteins in several regions of the mouse (Kreisel et al., 2010; Kinger et al., 2012). Bioluminescence imaging techniques allow visualization and longitudinal assessment of different white blood cell populations across both acute and chronic inflammatory phases (Tseng and Kung, 2013). However, both of these imaging techniques require contrasting dyes to evaluate specific molecular factors involved during inflammation. An alternative approach to assess an inflammatory response is to observe morphological and physiological changes in the tissue, including swelling and lymphatic vessel recruitment (Lachance et al., 2013). Tissue swelling is often observed during inflammation due to increased vascular permeability and accumulation of white blood cells. Lymphatic vessels are recruited locally to transport the fluid and extravasated white blood cells to local lymphoid organs and relieve edema (Zgraggen et al., 2013). To our knowledge, no study has been conducted to assess inflammation using these parameters during longitudinal arteriogenesis, or to link the vascular remodeling process to changes in tissue morphology over time.

Optical Coherence Tomography (OCT) produces large-scale (millimeters) cross-sectional morphological views of microstructure *in vivo* with micron level resolution (Tomlins and Wang, 2005). It is useful in showing progression of tissue swelling and thickness changes over time after lipopolysaccharide-induced inflammation in a mouse ear model (Kim et al., 2015). OCT-based microangiography (OMAG) adds the ability to image functional blood perfusion down to the capillary flow level (Wang et al., 2007; Wang, 2010; Wang and Hurst, 2007; An et al., 2010; Baran and Wang, 2016). Additionally, Doppler OMAG (DOMAG) detects a wide range of axial blood flow velocity within vessels (Wang and An, 2009; Shi et al., 2013), which reveals detailed vasodynamics information about blood flow during arteriole obstruction. This technique has been applied to the longitudinal study of microcirculation changes during wound healing in the mouse ear pinna (Wang et al., 2014), and to the *in vivo* examination of mouse cerebral vasodynamics in response to ischemic stroke (Jia et al., 2011; Baran et al., 2015). Moreover, the recently developed OCT-based lymphangiography (OLAG) has successfully been applied to produce lymphangiograms of post-depilation mouse ears (Qin et al., 2015, 2016), and within human skin and areola (Baran et al., 2016).

In this paper, we present the ability of OCT-based techniques to monitor arteriogenesis in mouse ear pinna and brain. Due to its relatively simple vessel networks compared to many other tissue beds and ease of access for optical imaging, we first elected to use the mouse ear as a model to investigate the capability of OCT based

techniques to delineate vessel remodeling during arteriogenesis, as well as the associated tissue responses due to inflammation. We then tested the method on the brain, which has a more complex vascular pattern, and demonstrated the potential of OMAG/OCT to image arteriogenesis in mouse cerebral cortex after focal ischemic stroke.

2. System and methods

2.1. Animal preparation and procedure

All animal procedures performed in this study were approved by the Institutional Animal Care and Use Committee (IACUC) of the University of Washington. All mice were anesthetized with 1.5–2.0% isoflurane (0.2 L/min O_2, 0.8 L/min air) through a nose cone and were provided with thermal support while anesthetized.

For the mouse ear study, five hairless SKH-1E mice (21–23 g) purchased from Charles River Laboratory were imaged under 1.5%–2.0% isoflurane anesthesia, resting on a heated platform. The mouse ear was immobilized using a piece of double-sided tape with the dorsal side facing upwards onto a stage that minimizes motion caused by breathing and heartbeats. A 5×5 mm region-of-interest (ROI) was selected that covered at least two major pinna artery branches with potential collateral arterioles in between. The ROI was covered with a drop of mineral oil and a round 0.15 mm thick coverglass as a coupling medium to mitigate strong reflection from the pinna surface. A baseline image of the ROI was acquired using OMAG and DOMAG. To induce arterial obstruction in the ear, one of the arteries in the ROI was selected and transected using microsurgical scissors just proximal to the ROI. Much care was taken during artery cutting to minimize possible damage to the surrounding tissue. The ROI was imaged immediately following artery transection. To observe the chronic stages of arteriogenesis, OMAG and DOMAG imaging were performed again at day 1, 4, 7 after artery transection.

For mouse brain imaging, four C57BL/6 mouse (weighing 23–25 g) was used. Under isoflurane anesthesia, the mouse received a 4×4 mm diameter craniotomy 1.5 mm posterior and lateral to bregma (Li et al., 2014), and a round 5×5 mm diameter (0.15 mm in thickness) cover glass was placed over the cortex to replace the cranium. The cranial window covers the cerebral territories supplied by the anterior cerebral artery (ACA), middle cerebral artery (MCA), and arteriolo-arteriolar anastomoses (AAA). Baseline imaging of the cerebral vasculature through the cranial window was taken by OMAG and DOMAG. After the baseline imaging, while still under anesthesia, the mouse received an intra-luminal filament MCA occlusion (MCAO) surgery, where a 6-0 monofilament was slowly advanced through internal carotid artery toward the cranial base until MCA was occluded (Baran et al., 2015). Imaging was then performed during a 60-min occlusion period. To visualize changes in blood flow after MCA reperfusion, the inserted filament was removed and imaging was immediately performed.

2.2. System configuration

A fiber-based spectral domain (SD-OCT) system was used for the experiments, in which a superluminescent diode (Thorlabs Inc., Newton, NJ, USA) was employed as the light source, which has the central wavelength of 1340 nm and bandwidth of 110 nm that provided a ~7 μm axial resolution in the air (~5 μm in tissue if the refractive index of tissue is taken as 1.35). In the sample arm, 10× scan lens (Thorlabs Inc., Newton, NJ, USA) was used to achieve ~10 μm lateral resolution with 0.12 mm depth of fields. The output light from the interferometer was routed to a home-built spectrometer, which had a designed spectral resolution of ~0.141 nm that provided a detectable depth range of ~3 mm on each side of the zero delay line in air. The system had an imaging speed of 92,000 A-scans per second, and a measured dynamic range of 105 dB with the incident light power of 3.5 mW at sample surface.

2.3. Scanning protocol

In the OMAG scanning protocol to visualize the volumetric microvasculature (An et al., 2010), each B-frame consisted of 400 A-lines. The imaging rate was 180 fps. In the slow axis (C-scan), a total number of 3200 B-frames with 8 repetitions in each location were performed for mouse ear imaging, and a total number of 2000 B-frames with 5 repetitions for mouse brain imaging. The OMAG volume dataset was collapsed into an *enface* maximum intensity projection (MIP) to represent the vessel network. A mosaic of 9 MIP images was made for each ROI.

To image the blood flow velocity of functional vessels, DOMAG scanning protocol was applied, and the blood flow velocity (axial component) was calculated from the phase difference between the OCT inter A-lines (Shi et al., 2013). The B-scans rates were empirically set to 3 and 6 frames per second (fps) for the mouse pinna and brain measurements, respectively, depending on their different blood flow speed. A mosaic of 9 MIP images was used to cover the entire 5×5 mm ROI.

2.4. Tissue inflammation analysis

Tissue inflammation analysis was performed based on lymphatic vessel visualization and mouse ear thickness change. We developed an automatic segmentation algorithm for the extraction of lymphatic vessel from the OCT microstructure image, based on the fact that the lymph fluid is optically transparent, thus giving optical signals near the system noise floor (Zhi et al., 2012). Prior to the algorithm, to mitigate the shadow cast by blood vessel and relative weak signal intensity in deeper tissue due to the light attenuation along depth, we pre-processed the microstructure images to remove the shadow cast and enhance the contrast (Qin et al., 2015, 2016). Then, we applied the adaptive threshold segmentation algorithm to extract lymphatic vessels. In the program, an adaptive threshold was first calculated by the intensity of the pixels within a local window around a target pixel to perform binarization operation. The window size was designed to be adjustable according to local lymphatic vessel size. If the intensity of target pixel was lower than the adaptive threshold, then that target pixel was judged to belong to lymphatic vessel, and assigned to a value of 1; otherwise it was assigned to 0. Finally, the processing was performed frame by frame for the whole 3D dataset to obtain a final 3D data volume, showing the lymphatic vessels only. Additionally, tissue swelling and thickness change induced by inflammation was evaluated by OCT structural imaging using the datasets acquired above. We applied a unique segmentation technique (Yin et al., 2014) to OCT cross-sectional images to extract the layer between dermis and cartilage (the layer of arteriole transection) for tissue thickness change analysis.

3. Results

Volumetric microvasculature of entire ROI in the mouse ear pinna is presented in Fig. 1A, covering three major artery branches and pre-existing collateral arterioles. The site of arterial transection is proximal to the right artery branch in the ROI, and is marked with red asterisk. After arterial transection, collateral arterioles are activated to retain the blood flow downstream to the transection. One collateral arterioles undergoing major remodeling is selected to take diameter and velocity measurement. Another arteriole further away to the transection site is measured as control. The magnitudes of collateral arteriole wall expansion are quantitatively presented

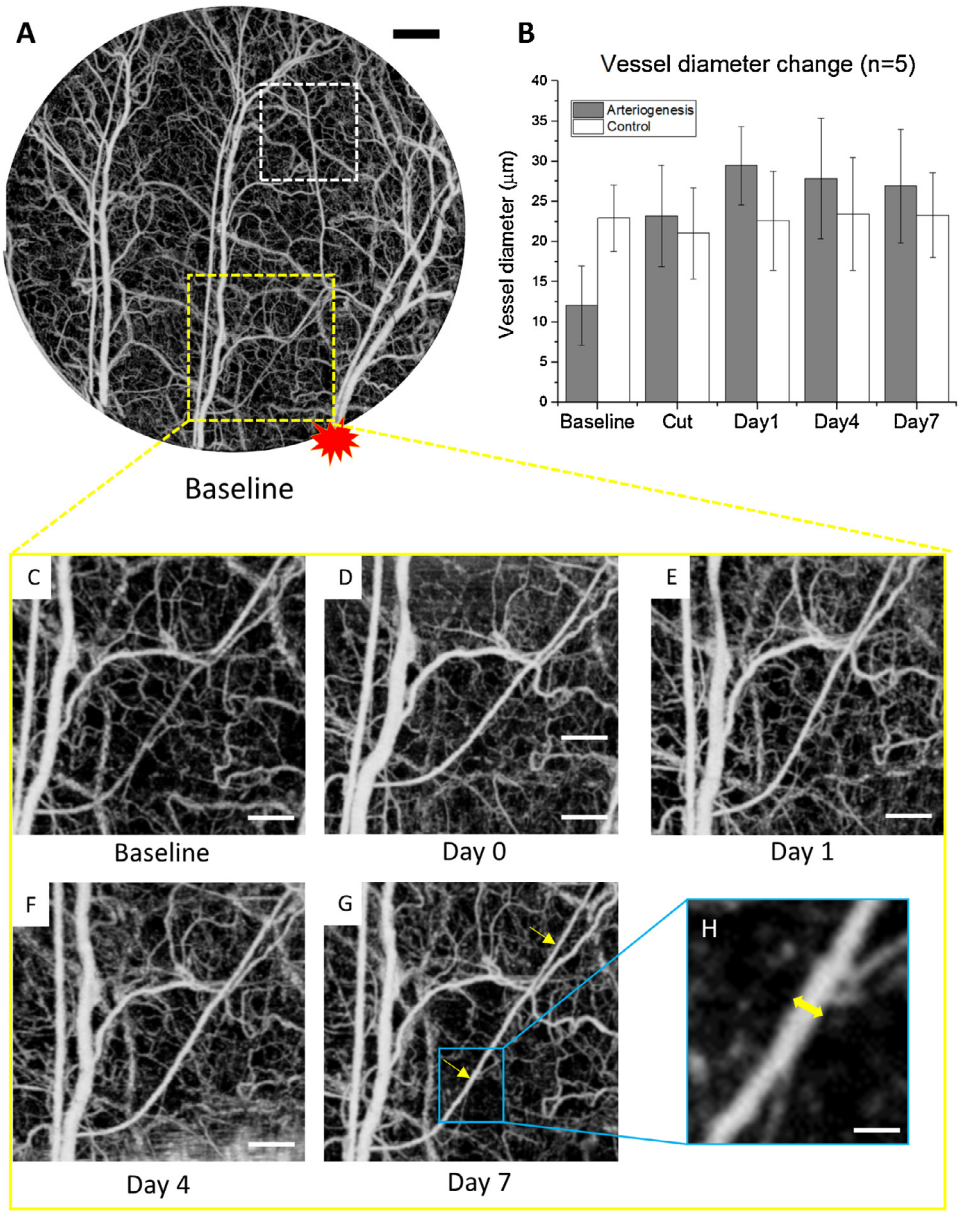

Fig. 1. Collateral arteriole morphology changes during longitudinal arteriogenesis in mouse ear.
(A) *En face* maximum intensity projection (MIP) of OMAG of the layer between epidermis and cartilage in mouse ear pinna flap within the area of interest at baseline. The red asterisk marks the relative location of artery transection. The yellow square indicates the location of the arteriole that underwent arteriogenesis, and the white square indicates the control region. (B) Vessel diameter change of the selected collateral arterioles in 7-day period. Error bars represent the standard error of the mean (SEM) of the arteriole diameters in 5 different animals. (C)–(G) Vessel morphology change of one of the major collateral arterioles being remodeled after artery transection. Two yellow arrows in (G) represent the two locations for diameter measurement. The yellow short line in (H) represents the diameter measurement of one location. Scale bars represent 500 μm, 250 μm, and 50 μm in (A), (C–G), and (H), respectively (For interpretation of the references to color in this figure legend, the reader is referred to the web version of this article.).

with vessel diameter change among 5 animals in Fig. 1B, where the targeted collateral arterioles have an increased diameter immediately following vessel transection, reaching peak at day 1, whereas the arteriole at the control region showing no significant diameter change.

Close-up views of the vessel morphology change with arteriogenesis are shown with Fig. 1C–G at baseline, cut (immediately after transection), day 1, day 4, and day 7, respectively. For diameter measurement, two locations on the arteriole was measured to yield an average diameter value for each time point (Fig. 1G). In the measurement from OMAG images using a MATLAB graphical user interface, the full width at half maximum of the normalized intensity profile across the collateral vessel is calculated with ~2 μm/pixel resolution, resulting in the vessel diameter (Fig. 1H). The arteriole at the control region are measured based on the same method.

Blood flow velocity changes in the functional collateral arterioles were measured based on red blood cell axial velocities detected in DOMAG. Bidirectional velocity maps of a representative mouse ear pinna are presented in Fig. 2A–E with upward direction coded green and downward direction coded red. Few out-of-range flows are observed as phase-wrapped signals, seen as yellow color (combination of red and green). For each arteriole, two locations of axial velocity are measured to average. We measured the arteriogenic collateral vessels as well as the arterioles with no active remodeling as control. At the arteriogenesis region, an enhancement of the

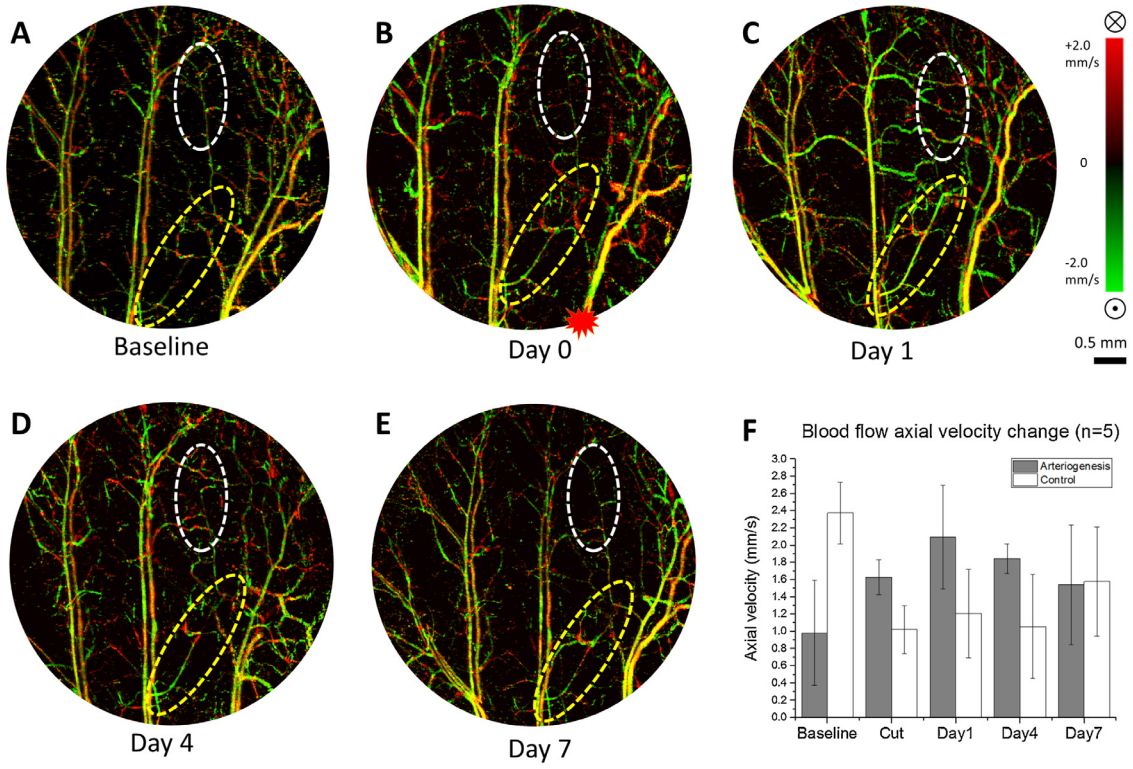

Fig. 2. Collateral arteriole blood flow axial velocity change during arteriogenesis in mouse ear.
(A)–(E) *En face* MIP of DOMAG of the whole depth of mouse ear pinna within the area of interest at baseline, cut, day 1, day 4, day 7, respectively. The red asterisk in (B) marks the location of artery transection. Vessels are color coded with green and red in regards to flow directions. Yellow is a combination of two colors. Color bar represents blood flow axial velocity in range of ±2.0 mm/s. Note the yellow color appearance is due to the fusion of red and green colors, caused by the 2pi ambiguity in the Doppler phase measurement of fast blood flows when applying Doppler principle. (F) Blood flow axial velocity change of the arterioles within the yellow circles (arteriogenesis), and white circle (control). Error bars represent the SEM of the mean axial velocity in 5 different animals. Scale bar represents 0.5 mm in all DOMAG images (For interpretation of the references to color in this figure legend, the reader is referred to the web version of this article.).

arteriole velocity signal is observed immediately after artery transection (cut), and the velocity reached a peak on day 1, whereas the controlled arteriole distal to the transection site showing reduced blood flow velocity and poor recovery over time (Fig. 2F).

Inflammation plays an important role during arteriogenesis for growth factor recruitment and breaking down of extracellular matrix (Schaper and Scholz, 2003). We investigated whether the magnitude of inflammation has a similar time course as the vessel remodeling by observing lymphatic structure and tissue thickness change. We applied OLAG technique to extract the fluid-filled lymphatic signal from OCT cross-sectional structures, and created a merged channel showing lymphatic vessel networks in light blue and OCT angiogram in red simultaneously (Fig. 3A–E). Lymphatic vessels provide paths for inflammatory cells to exit the inflammatory tissue. The appearance of lymphatic vessels in close proximity to the collateral arterioles undergoing arteriogenesis further proved the active inflammatory cell trafficking during arteriogenesis. As lymphatic vessels take up more fluid they become more apparent to OCT, creating a more continuous network. As a result, the most continuous lymphatic vessel network is observed at day 1 (Fig. 3C).

After artery transection, the ear pinna swells due to a neutrophil-dominant infiltration and edema from increased vascular permeability (Wright et al., 2010), and the resulting tissue thickness change is another parameter to assess inflammation progression. Tissue thickness change measurements at both lymphatic-dense area and control area were performed among 5 mice using a structural segmentation technique (Yin et al., 2014). The most severe tissue deformation was observed locally to the inflammatory tissue at day 1, and this trend is not observed at the control area where there is no or less lymphatic vessels (Fig. 3F). Both lymphatic vessels and mouse ear thickness consistently revealed local inflammation progression in regards to arteriogenesis.

OMAG/DOMAG technique also has the ability in monitoring collateral circulations in the mouse cerebral cortex during stroke. A demonstration of arteriogenesis in mouse cerebral cortex is presented in Fig. 4. Cerebral pial vessel structures and the corresponding bidirectional axial blood flow velocity of pial vessels are given in baseline, occlusion (MCAO), and reperfusion. ACA and MCA supplying territories are distinguished by blood flow directions at baseline Discontinuities in vessel connectivity are observed at AAA in DOMAG due to the slow oscillating blood flow at this preserved vascular region (Toriumi et al., 2009), but vessel structure remains present in OMAG due to the high movement sensitivity of OMAG. During MCAO, the pre-existing AAA became activated and turned into functioning collateral arterioles (Fig. 4B and E).

A reversal of the blood flow direction can be also observed at the MCA branches through collateral circulation. After reperfusion, blood flow in MCA is restored, but the AAA remain in function.

4. Discussion

Two distinct forms of vascular remodeling can be observed after blood flow obstruction: angiogenesis and arteriogenesis. According to Schaper and Scholz (2003), *arteriogenesis* is a process whereby a pre-existing arteriole from the resistant vessel class matures into an artery of conductive vessel class, whereas *angiogenesis* is a process where new capillaries sprout from pre-existing capillaries. Both types of adaptive vessel growth play an important role in reducing

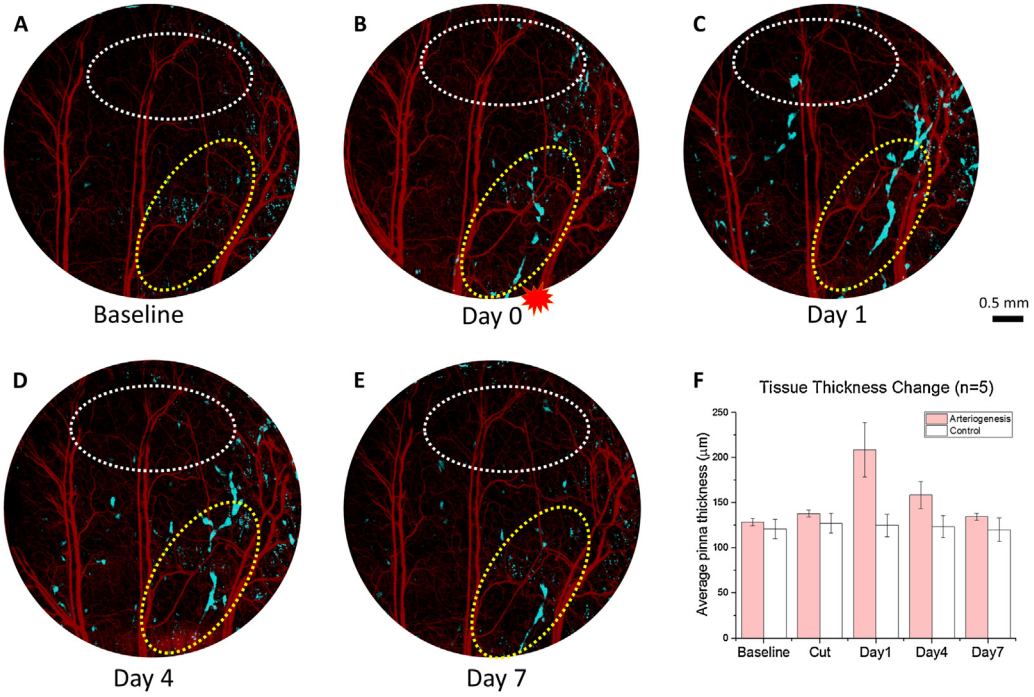

Fig. 3. Local inflammation progression during arteriogenesis.
(A)–(E) Merged images of lymphatic vessels (blue) and vasculature (red) in three dimensions of the mouse ear layer between epidermis and cartilage at baseline, cut, day 1, day 4, and day 7, respectively. The red asterisk in (B) marks the location of artery transection. Yellow circles indicate the area of local inflammation signified by lymphatic vessel formation, and white circles indicate the control region with no or less lymphatic vessels. (F) Average tissue thickness change of the pinna (between epidermis and cartilage) at both yellow (arteriogenesis) and white (control) circles was measured. Error bars represent the SEM of the thickness from 5 mouse ears. Scale bar represents 0.5 mm in all 5 images (For interpretation of the references to color in this figure legend, the reader is referred to the web version of this article.).

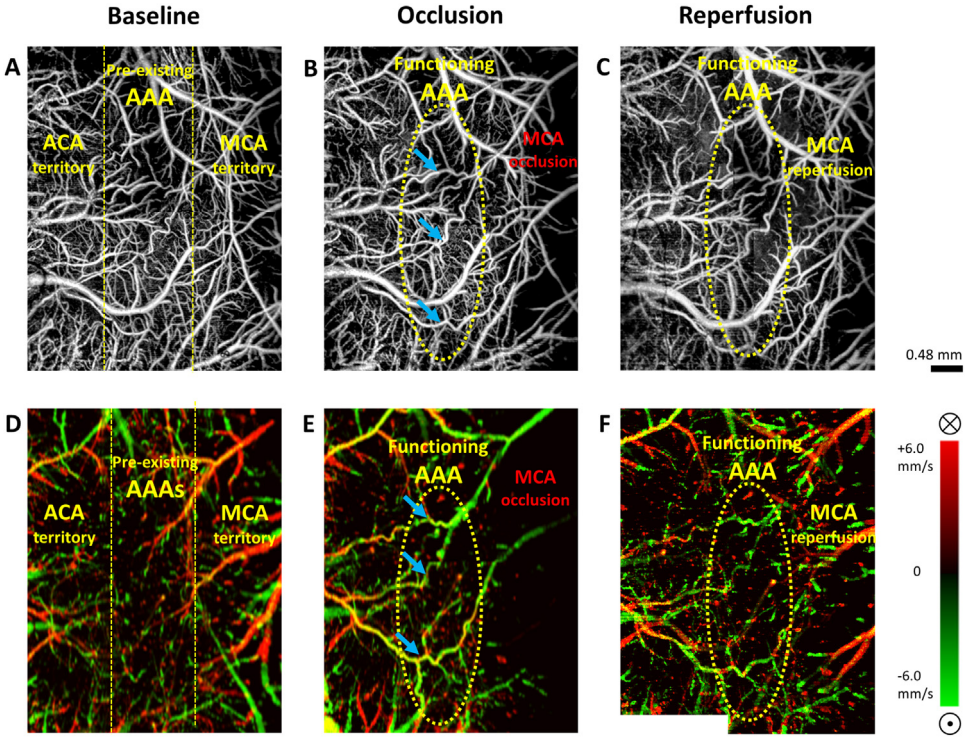

Fig. 4. Arteriogenesis at cerebral anastomoses in mouse brain during stroke.
(A)–(C) *En face* MIP of OMAG within 100 μm depth from the cortical surface at baseline, occlusion (MCAO), reperfusion, respectively. (D)–(F) *En face* MIP of DOMAG with directional blood flow axial velocity distribution color-coded, corresponding to OMAG images above. Color bar represents blood flow axial velocity in range of ±6.0 mm/s. Blue arrows identified three of the functioning anastomoses in relation to their positions in OMAG and DOMAG during occlusion. ACA: anterior cerebral artery. MCA: middle cerebral artery. AAA: arteriolo-arteriolar anastomoses between MCA and ACA. Scale bar represents 0.48 mm in all images (For interpretation of the references to color in this figure legend, the reader is referred to the web version of this article.).

ischemic damage and repairing tissue. However, only arteriogenesis provides an equivalent response to blood flow deficits caused by arterial occlusion given that capillaries are unable to replace larger conductive arteries (Schaper and Buschmann, 1999).

Occlusive vascular diseases remain a major cause of death and morbidity in industrialized societies. For decades, efforts have been made to develop therapeutic approaches that stimulate self-curing mechanisms within the body. Since collateral arterioles can function as "natural bypasses" in maintaining regional blood flow and offsetting the adverse effect of tissue ischemia, stimulation of arteriogenesis has become a potential candidate for the treatment of occlusive vascular disease (van Royen et al., 2001). However, the complex process of arteriogenesis is not fully understood. Previous identification of collateral vessel structural change relying on histology is not sufficient to observe vasodynamics over time, and may present difficulties when evaluating the effectiveness of an arteriogenic factor. A powerful imaging technique that provides consistent quality of vasculature and flow status, desirably non-invasive, would improve our understanding of the mechanisms of arteriogenesis and contribute to the development of new therapies.

OCT-based angiography is increasingly becoming an important angiographic technique due to its ability to generate volumetric microvascular networks of biological tissue with excellent resolution (1–10 μm resolution) without a need of exogenous contrast agent. Numerous OCT angiography algorithms have recently been proposed for microvascular imaging, including optical microangiography (OMAG), phase variance techniques, split-spectrum techniques, etc. A recently published review article has evaluated methods and algorithms for OCT-based angiography based on three metrics obtained by each algorithm (Zhang et al., 2015). As a result of the comparison, OMAG, which is an algorithm based on complex OCT signal, delivers the best performance overall, in aspects of vessel connectivity, contrast, and signal-to-noise ratio (SNR). Additionally, the review also suggests a faster processing time using OMAG algorithm which reduces overall computational cost.

In this study, we applied the high-resolution OMAG technique to reveal *in vivo* changes in arterioles in a mouse ear and brain, observing key elements of the process of arteriogenesis, including alteration in collateral vasculature morphology, vessel outward growth, and blood flow velocity change. In the longitudinal mouse ear study, we observed peaking in vessel diameter expansion and blood flow velocity increase at day 1 but not immediately after artery transection (Figs. 1B, 2E). According to the literature, arteriogenesis involves altered fluid shear stress caused by arterial obstruction, which initiates a complex cascade of molecular and cellular events leading to increased vessel lumen and wall thickness (Heil et al., 2006). This is not a process of passive dilation but active proliferation and remodeling which requires time to develop. This peak growth time observed in our study is consistent with reports that the active growth phase in arteriogenesis occurs between 12 and 24 h (Buschmann et al., 2003). We also investigated whether the magnitude of inflammation has a similar time course as the vessel remodeling by observing lymphatic structure and edema induced tissue thickness change. From our result, both local lymphatic vessel activity and tissue thickness reach the greatest value at day 1 (Fig. 3), sharing a similar time course with the surrounding vascular remodeling.

It is important to mention that after artery transection, a great deal of collateral arterioles were being actively remodeled to retain the downstream blood flow. Hence, artery structure downstream at the transection point can be better preserved in OMAG angiogram even immediately after the transection (Fig. 3B), as well as a quick restoration in the blood flow velocity downstream to transection point shown in DOMAG (Fig. 2B). For statistics, one of the major collateral arterioles was picked randomly from each mouse for diameter and blood flow velocity measurement.

The OMAG/DOMAG technique presents a potential in monitoring collateral circulations in mouse cerebral cortex during stroke. At baseline, the ultra-sensitive OMAG reveals a complete cerebral pial vessel angiogram (Fig. 4A) regardless of a velocity discontinuity at anastomoses in DOMAG (Fig. 4D) due to the slow oscillating blood flow at this preserved vascular region. This feature will be useful in identifying the location of vessel connections prior to ischemic injury and predict collateral circulation outcome. In the meanwhile, DOMAG presents a bidirectional axial blood flow velocity map that differentiate three kinds of vascular supplying territories: ACA, MCA, and dually supplied AAA (Fig. 4D). It also captures territory shift during occlusion and reperfusion, which can provide guidance in the study of hemodynamic homeostasis at the T-junctions during ischemic injury. In this current study, survival experiments of MCAO were not performed, however, application of OMAG imaging techniques to a longitudinal stroke model may yield additional insights to the progression of arteriogenesis after cerebral arterial occlusion. This model could be useful to develop novel therapies that stimulate arteriogenesis to improve cerebral blood flow after stroke.

In addition to cerebral vascular visualization, a cross-sectional structural thickness information obtained from OCT images may be potentially applied in cerebral edema assessment. Cerebral edema, also referred to as brain swelling or intracranial pressure, can result from brain trauma or from ischemic stroke and inflammation due to meningitis or encephalitis (Raslan and Bhardwaj, 2007). The edema takes up brain's extracellular space resulting in brain tissue swelling and thickness change, which could compromise the regional or global blood flow. The consequences of cerebral edema can be lethal, and managing cerebral edema development is critical to prevent secondary neuronal injury. A brain tissue thickness evaluation provided by OCT may be a great non-invasive tool to guide the management of cerebral edema development and regional CBF maintenance during and after ischemic injury.

One limitation to the technique described here is the possibility for inconsistencies in measured axial velocity. Small changes in sample position between imaging sessions could affect the observed axial velocity because this measure is dependent on the angle between the beam and sample surface. This concern highlights one of the major challenges in longitudinal DOMAG analysis in arteriogenesis, as the vessels orient in various angles inside the biological tissue. We have attempted to minimize the potential for this error by carefully orienting the sample frame the same at each imaging session. However, further study will be needed to refine the sample placement to improve the reliability of axial velocity (*e.g.*, using a goniometer stage with a large angular range or increase the sample number in the statistics).

5. Conclusion

In this study, we have demonstrated the feasibility of an OCT-based OMAG technique to image *in vivo* arteriogenesis in mouse ears and delineate cerebral collateral circulation in the mouse brain. We have shown that OMAG is useful to reveal comprehensive information during arteriogenesis, including the active expansion of collateral vessels and increased blood flow. Our results from the mouse ear pinna have shown that the time course of collateral vessel diameter and velocity change agree with previous reports that the active growth phase of arteriogenesis occurs between 12 and 24 h after induction by vessel occlusion. The OCT technique also provides the ability to assess tissue inflammation based on cross-sectional structural images and lymphangiograms. These techniques can be applied to multiple tissue types, and have the potential to guide future experimental studies of arteriogenesis

stimulation therapies for occlusive vascular diseases, including stroke.

References

An, L., Qin, J., Wang, R.K., 2010. Ultrahigh sensitive optical microangiography for in vivo imaging of microcirculations within human skin tissue beds. Opt. Express 18 (8), 8220–8228.

Baran, U., Wang, R.K., 2016. Review of optical coherence tomography based angiography in neuroscience. Neurophotonics 3 (1), 010302.

Baran, U., Li, Y., Wang, R.K., 2015. Vasodynamics of pial and penetrating arterioles in relation to arteriolo-arteriolar anastomosis after focal stroke. Neurophotonics 2 (2), 025005.

Baran, U., et al., 2016. OCT-based label-free in vivo lymphagiography within human skin and areola. Sci. Rep. 6, 21122.

Buschmann, I.R., et al., 2001. GM-CSF: a strong arteriogenic factor acting by amplification of monocyte function. Atherosclerosis 159 (2), 343–356.

Buschmann, I., Katzer, E., Bode, C., 2003. Arteriogenesis-is this terminology necessary? Basic Res. Cardiol. 98 (1), 1–5.

Demicheva, E., Hecker, M., Korff, T., 2008. Stretch-induced activation of the transcription factor activator protein-1 controls monocyte chemoattractant protein-1 expression during arteriogenesis. Circ. Res. 103 (5), 488–484.

Heil, M., Eitenmüller, I., Schmitz-Rixen, T., Schaper, W., 2006. Arteriogenesis versus angiogenesis: similarities and differences. J. Cell Mol. Med. 10 (1), 45–55.

Hu, S., Maslov, K., Wang, L.V., 2009. Noninvasive label-free imaging of microhemodynamics by optical-resolution photoacoustic microscopy. Opt. Express 17 (9), 7688–7693.

Jia, Y., Li, P., Wang, R.K., 2011. Optical microangiography provides an ability to monitor responses of cerebral microcirculation to hypoxia and hyperoxia in mice. J. Biomed. Opt. 16 (9), 096019.

Kim, B., et al., 2015. In vivo visualization of skin inflammation by optical coherence tomography and two-photon microscopy. Biomed. Opt. Express 6 (7), 2512–2521.

Kinger, A., et al., 2012. Complex morphology and functional dynamics of vital murine intestinal mucosa revealed by autofluorescence 2-photon microscopy. Histochem. Cell Biol. 137 (3), 269–278.

Kreisel, D., et al., 2010. In vivo two-photon imaging reveals monocyte-dependent neutrophil extravasation during pulmonary inflammation. PNAS 107 (42), 18073–18078.

Lachance, P.-A., Hazen, A., Sevick-Muraca, E.M., 2013. Lymphatic vascular response to acute inflammation. PLoS One 8 (9), e76078.

Li, Y., Baran, U., Wang, R.K., 2014. Application of thinned-skull cranial window to mouse cerebral blood flow imaging using optical microangiography. PLoS One 9 (11), e113658.

Liu, J., et al., 2014. Vascular remodeling after ischemic stroke: mechanisms and therapeutic potentials. Prog. Neurobiol. 115, 138–156.

Meisner, J.K., Price, R.J., 2010. Spatial and temporal coordination of bone marrow-derived cell activity during arteriogenesis: regulation of the endogenous response and therapeutic implications. Microcirculation 17 (8), 583–599.

North, K.A., Sanders, A.G., 1958. The development of collateral circulation in the mouse's ear. Circ. Res. 6 (6), 721–727.

Qin, W., Baran, U., Wang, R.K., 2015. Lymphatic response to depilation-induced inflammation in mouse ear assessed with label-free optical lymphangiography. Lasers Surg. Med. 47 (8), 669–676.

Qin, W., et al., 2016. In vivo monitoring of microcirculation in burn healing process with optical microangiography. Adv. Wound Care 5 (8), 332–337.

Raslan, A., Bhardwaj, A., 2007. Medical management of cerebral edema. Neurosurg. Focus 22 (5), e12.

Schaffer, C.B., et al., 2006. Two-photon imaging of cortical surface microvessels reveals a robust redistribution in blood flow after vascular occlusion. PLoS Biol. 4 (2), e22.

Schaper, W., Buschmann, I., 1999. Arteriogenesis versus angiogenesis: two mechanisms of vessel growth. News Physiol. Sci. 14 (3), 121–125.

Schaper, W., Scholz, D., 2003. Factors regulating arteriogenesis. Arterioscler. Thromb. Vasc. Biol. 23 (7), 1143–1151.

Shi, L., Qin, J., Reif, R., Wang, R.K., 2013. Wide velocity range Doppler optical microangiography using optimized step-scanning protocol with phase variance mask. J. Biomed. Opt. 18 (10), 106015.

Tomlins, P.H., Wang, R.K., 2005. Theory, developments and application of optical coherence tomography. J. Phys. D: Appl. Phys. 38 (15), 2519–2535.

Toriumi, H., et al., 2009. Dually supplied t-juntcions in arteriolo-arteriolar anastomosis in mice: key to local hemodynamic homeostasis in normal and ischemic states? Stroke 40 (10), 3378–3383.

Tseng, J.-C., Kung, A.L., 2013. In vivo imaging method to distinguish acute and chronic inflammation. J. Visualized Exp. 78, e50690.

van Royen, N., et al., 2001. Stimulation of arteriogenesis: a new concept for the treatment of arterial occlusive disease. Cardiovasc. Res. 49 (3), 543–553.

Wang, R.K., An, L., 2009. Doppler optical microangiography for volumetric imaging of vascular perfusion in vivo. Opt. Express 17 (11), 8926–8940.

Wang, R.K., Hurst, S., 2007. Mapping of cerebrovascular blood perfusion in mice with skin and cranium intact by optical microangiography at 1300 nm wavelength. Opt. Express 15 (18), 11402–11412.

Wang, R.K., et al., 2007. Three dimensional optical angiography. Opt. Express 15 (7), 4083–4097.

Wang, Z., et al., 2012. Dynamic change of collateral flow varying with distribution of regional blood flow in acute ishcemic rat cortex. J. Biomed. Opt. 17 (12), 125001.

Wang, H., et al., 2014. Multimodal optical imaging can reveal changes in microcirculation and tissue oxygenation during skin wound healing. Lasers Surg. Med. 46 (6), 470–478.

Wang, R.K., 2010. Opical microangiography: a lavel free 3D imaging technology to visualize and quantify blood circulation within tissue beds in vivo. IEEE J. Sel. Top. Quantum Electron. 16 (3), 545–554.

Wright, H.L., Moots, R.J., Rucknall, R.C., Edwards, S.W., 2010. Neutrophil function in inflammation and inflammatory diseases. Rheumatology 49 (9), 1618–1631.

Yin, X., Choa, J.R., Wang, R.K., 2014. User-guided segmentation for volumetric retinal optical coherence tomography images. J. Biomed. Opt. 19 (8), 086020.

Zgraggen, S., Ochsenbein, A.M., Detmar, M., 2013. An important role of blood and lymphatic vessels in inflammation and allergy. J. Allergy 2013, 672381.

Zhang, A., Zhang, Q., Chen, C., Wang, R.K., 2015. Methods and algorithms for optical coherence tomography-based angiography: a review and comparison. J. Biomed. Opt. 20 (10), 100901.

Zhi, Z., Jung, Y., Wang, R.K., 2012. Label-free 3D imaging of microstructure, blood, and lymphatic vessels within tissue beds in vivo. Opt. Lett. 37 (5), 812–814.